Indentation of a layer on foam substrate

A.M. Boyce , H.C. Tankasala , N.A. Fleck

PII: S0020-7403(18)33094-7
DOI: https://doi.org/10.1016/j.ijmecsci.2018.10.038
Reference: MS 4594

To appear in: *International Journal of Mechanical Sciences*

Received date: 19 September 2018
Revised date: 16 October 2018
Accepted date: 17 October 2018

Please cite this article as: A.M. Boyce , H.C. Tankasala , N.A. Fleck , Indentation of a layer on foam substrate, *International Journal of Mechanical Sciences* (2018), doi: https://doi.org/10.1016/j.ijmecsci.2018.10.038

Highlights

- Deep indentation response of a stiff, strong face sheet on foam substrate is analysed.
- Face sheet undergoes elastic bending (at shallow indentation), then elastic stretching followed by plastic stretching (at moderate to deep indentation).
- Membrane stresses in the face sheet elevate the indentation load significantly.
- Analytical model based on load diffusion principles suitably captures these observations.
- It highlights the role of material yield strain on the indentation resistance of bi-layers.
- An alternative collapse mode is observed in sandwich beams under 3-point bending; hardening is absent in this case.

Indentation of a layer on foam substrate

A M Boyce†, H C Tankasala*,†, and N A Fleck
Cambridge University Engineering Department, Trumpington St, CB2 1PZ, Cambridge, UK
18. September, 2018

Abstract

There is a practical need to elevate both the indentation strength and level of energy absorption of engineering foams by the addition of a stiff and strong face sheet for applications such as packaging and crash mitigation. In this study, the enhancement in plane strain indentation resistance of a polyvinyl chloride (PVC) foam by the presence of a polycarbonate (PC) face sheet is determined by experiment, finite element analysis and by an analytical model. Plane strain indentation is by a flat-bottom punch or by a cylindrical roller, and the strain distribution within the PC face sheet and in the foam substrate are measured by digital image correlation. With increasing indent depth, the face sheet bends and stretches elastically and then plastically until face sheet or substrate fail. The generation of membrane tension in the face sheet plays a major role in supporting the indentation load when the indent depth exceeds the thickness of the face sheet, and leads to a strong hardening behaviour beyond the initial collapse load for indentation. Finite element predictions of the full indentation response are based upon the measured tensile and compressive responses of the PVC foam and PC layer. An analytical model is developed by matching the stretching response of the PC face sheet to the indentation response of the underlying foam, with due consideration for load diffusion from membrane tension of the PC face sheet into the underlying foam substrate. The indentation model is calibrated by ancillary finite element simulations of the load diffusion problem, and they emphasise the role of a shear lag zone in dictating the large indentation resistance. The indentation response of the bi-layer is also compared with that of a sandwich beam in 3-point bending. Experiments, finite element simulations and an additional analytical model for indentation of the sandwich beam in 3-point bending reveal that strong hardening of the post-yield load versus displacement response is now absent, in contrast to that of the bi-layer. The lack of hardening in 3-point bending is traced to the relatively low value of plastic bending moment of the beam section.

Keywords: polymer foams, indentation, shear lag, 3-point bending, analytical model

1. Introduction

Polymeric foams typically exhibit a low ductility in tension (of only a few percent), but a high ductility in compression due to the formation of crush bands [1-3]. The indentation strength of polymeric foams is comparable to their uniaxial yield strength due to the volumetric compressibility of the foam, and the indentation strength is only

* Corresponding author. Email: hct30@cam.ac.uk
† These authors contributed equally to this work.

mildly sensitive to the indenter geometry, see [4-7]. For the practical application of foams to design for protective, energy absorbing packaging and for crash mitigation, it is desirable to enhance the indentation resistance of a foam substrate by the addition of a suitable face sheet.

The combination of a foam core and a stiff, strong face sheet commonly arises in sandwich construction: two stiff and strong face sheets are separated by a lightweight foam core. Sandwich panels are commonly used in flexural applications due to their low mass yet high stiffness and strength in bending. The early stage of plastic collapse of sandwich panels occurs by one of at least three competing mechanisms: face yield, core shear, and indentation [8-9]. The present experimental and theoretical study gives additional insight into the *indentation* mode of collapse, and addresses the case where indent depths exceed the face sheet thickness such that the face sheet undergoes membrane action prior to failure. This regime is of high practical significance; yet it has received little attention in the literature.

Our primary study is concerned with the plane strain indentation response of a single PC face sheet bonded to a PVC foam substrate upon a rigid foundation. PC is chosen due to its high tensile strength and ductility, and it finds common use in impact-resistant transparent components such as masks for eye protection. Our study complements the experimental investigation of Mohan et al. [10]: they observed a significant elevation in the axisymmetric indentation strength of a metallic foam due to the presence of a stainless steel face sheet.

1.1 Existing models for the indentation of a face sheet, on a foam substrate

To date, the plane strain indentation response of a layer on foam substrate has been concerned primarily with indentation depths that are less than the face sheet thickness. In such a case, membrane stresses within the top layer play little role. For example, Biot [11] analysed the indentation of an elastic layer, of thickness t and Young's modulus E_f, on an elastic half-space, whilst Hetenyi [12] simplified this problem by considering the idealised case of indentation of an elastic beam on an elastic spring foundation of modulus S by a line load P (per unit thickness). Hetenyi found that the indentation load P is related to the indent depth v by

$$P = 1.52 S^{3/4} t^{3/4} {E_f}^{1/4} v \tag{1}$$

Soden [13] extended the Hetenyi analysis for an elastic face sheet on a rigid, perfectly-plastic foundation of strength σ_{cy} to obtain

$$P = 2.1\, t^{3/4} {\sigma_{cy}}^{3/4} {E_f}^{1/4} v^{1/4} \tag{2}$$

Shuaeib and Soden [14] subsequently idealised the foam substrate by an elastic, perfectly- plastic foundation and more recently Pitarresi and Amorim [15] considered

the substrate to have a more general strain hardening characteristic as defined by a sequence of distributed springs.

Bostrom [16] analysed the indentation resistance of a rigid, perfectly-plastic face sheet of strength σ_{fy} resting on a rigid, perfectly-plastic foundation and loaded by a transverse point force P. An upper bound for the collapse load was obtained by assuming a mechanism of 3 plastic hinges in the face sheet, to give

$$P = 2t\sqrt{\sigma_{fy}\sigma_{cy}} \tag{3}$$

Ashby et al. [8] considered plane strain indentation of a metal face sheet (assumed as rigid, perfectly-plastic) on a metal foam core (also assumed to be rigid, perfectly-plastic) by a flat- bottom punch of width $2a$. They gave an upper bound solution for the indentation load due to formation of 4 plastic hinges (adjacent to the punch) in the face sheet as

$$P = 2t\sqrt{\sigma_{fy}\sigma_{cy}} + 2a\sigma_{cy} \tag{4}$$

Chen et al. [17], Bart-Smith et al. [18], and McCormack et al. [19] gave experimental support for this plastic collapse mechanism by performing 3-point and 4-point bend tests on sandwich beams. Whilst this mechanism exists at small indents (with respect to the face sheet thickness), it neglects the generation of membrane stretching within the face sheet at larger indent depths. The significance of such membrane stretching will be a focus of the present study.

Yu and Stronge [20] realized the interaction between plastic bending and stretching in the regime of large indentation depth for a rigid, perfectly-plastic face sheet on a rigid, perfectly-plastic foundation. Following an upper bound approach with an assumed velocity field, they obtained a 'membrane factor' to account for plastic stretching of the face sheet induced by large deflections. The indentation load P increases with the indent depth v in the stretching regime according to

$$P = 2\sqrt{2\sigma_{fy}\sigma_{cy}tv} \tag{5}$$

An alternative model was developed recently by Rubino et al. [21] based on experiments on Y-frame and corrugated core bi-layer made from stainless steel. The assumed collapse mechanism involves rotation of the face sheet about 4 plastic hinges, stretching of the face sheet between the inner and outer hinges, compressive yielding of the core, and shear deformation of the core (of depth c and shear strength τ_{cy}). The resulting indentation load versus displacement relation is

$$P = 2\sqrt{\sigma_{fy}\sigma_{cy}t(2v + t)} + c\tau_{cy} \tag{6}$$

More recent treatments of indentation on a foam substrate include combined analytical and finite element studies on the effect of plastic stretching of the face sheet due to large deflections [22-27]. Both Xiao et al. [23] and Xie et al. [24] used an upper bound approach by assuming a velocity field and assumed that the face sheets and core are rigid, perfectly-plastic. Thereby, Xie et al. [24] found the same collapse load as that given by (5). Upon including shear yielding of the core, Qin et al. [25] obtained a collapse load similar in form to (6) from their upper bound analysis. Qin and Wang [22] and Zhang et al. [26-27] modelled the response of end-clamped sandwich beams under large deflections in their finite element calculations.

Note that the above analyses, assuming rigid, perfectly-plastic behaviour, ignore elastic stretching of the top face sheet and elastic compliance of the foam core. It is anticipated that the role of elastic deformation is significant in bi-layers where each phase has a high value of yield strain, such as PC face sheets on a polymer foam core, as noted by Boyce et al. [28]. In order for membrane stresses to exist within the face sheet, there must be load transfer between the face sheet and the foam substrate. This problem of load diffusion between a strip and a substrate has a long and illustrious history, see for example Koiter [29] and Muki and Sternberg [30]. Here, we shall present a simple analytical model for membrane stretching of the face sheet during indentation, based on these classical ideas.

1.2 Scope of study

The deep indentation response of a polycarbonate (PC) face sheet adhered to a polyvinyl chloride (PVC) foam substrate (on rigid foundation) is measured. Digital image correlation (DIC) is used to probe the indentation mode as a function of increasing indent depth. The effects of indenter size and shape (flat-bottom punch versus cylindrical roller) and of specimen length upon the collapse response and failure mechanisms are also explored. The deformation response is modelled by finite element simulations and, together with the observations, a simplified analytical model is synthesised. The model assumes elastic membrane stretching of a face sheet on an elastic, perfectly-plastic foam foundation, and includes the role of shear lag between face sheet and foam substrate. The study ends with a comparison of the indentation response for a face sheet on foam substrate with that of a sandwich beam in 3-point bending. It is found that membrane stresses do not develop in the face sheet for the case of 3-point bending, and consequently the indentation response has negligible hardening post yield. An analytical model is developed to give direct insight into this alternative collapse mechanism.

2. Test method

2.1 Indentation test geometry

The indentation test setup is sketched in Fig. 1. The specimens comprised a DIAB Divinycell H200 PVC closed cell foam substrate and a Lexan 9030-112 PC top layer,

bonded together by a cyanoacrylate adhesive[‡]. In all cases, the face sheet thickness was $t = 1$ mm, the foam substrate thickness was $c = 100$ mm; both were of depth $b = 25$ mm into the page. The bottom face of the PVC foam was bonded by the cyanoacrylate adhesive to a steel plate of sufficient thickness $H = 50$ mm that the plate behaves in a rigid manner relative to that of the foam and face sheet. The steel-backed specimens were placed on the loading platen of a screw-driven tensile test machine.

A series of indent tests are listed in Table 1, and were performed as follows:

I. An initial basic study whereby the bi-layer (on steel support) was indented by a flat-bottom punch of width $2a = 4$ mm with a corner radius $\rho = 0.5$ mm, see Fig. 1. The indent velocity was $\dot{v} = 0.025$ mms^{-1}, and the overall length of the specimen was $\ell = 400$ mm, as listed in Table 1. Additionally, an indentation test was performed on a foam substrate absent the PC layer to provide insight into the indentation response of a foam layer as the reference case.
II. The effect of indenter *size* (relative to face sheet thickness) was determined by employing 2 additional flat-bottom punches, of width $2a = 2$ mm and 10 mm, with corner radius $\rho = 0.5$ mm.
III. The sensitivity of indentation response to *head shape* was explored by performing tests at $\dot{v} = 0.025$ mms^{-1} and $\ell = 400$ mm using circular rollers of radius $r = 1, 2,$ and 5 mm.
IV. *Rate sensitivity* was determined by performing additional tests using the flat-bottom punch of width $2a = 4$ mm, and $\dot{v} = 0.0025$ mms^{-1} and 0.25 mms^{-1}.
V. The overall specimen *length* was decreased from $\ell = 400$ mm to $\ell = 50$ mm in order to determine the effect of specimen length on the development of membrane action in the face sheet. This test also made use of the flat-bottom punch of width $2a = 4$ mm, and an indent velocity of $\dot{v} = 0.025$ mms^{-1}.

In each case, 3 repeat experiments were carried out on each specimen. A 3D Digital Image Correlation (DIC) system[§] was used to visualize and measure the surface strain field during the indentation tests. Prior to testing, a matt white spray paint base coat was applied to the specimen followed by a black paint to generate a fine black speckle pattern. The white base ensured that any reflections from variation in the texture of the underlying specimen were minimised, thereby allowing accurate tracking of the displacement of each black speckle. Images were acquired at a frequency of 0.33 Hz and a resolution of 4096 x 3072 pixels during the experiments; these images were subsequently used to produce the in-plane strain contour maps using the correlation software of the DIC system.

2.2 Test materials

The uniaxial tensile and compressive stress versus strain responses of the PC face sheet and of the PVC foam were measured; these are plotted as nominal (engineering) quantities in Fig. 2. The initial response of PC is linear elastic with a Young's modulus

[‡] Henkel Loctite 401, low viscosity, fast curing adhesive.
[§] Aramis, GOM GmbH and GOM correlate software.

$E_f = 2$ GPa, at a strain rate of 10^{-4} s^{-1}. Tensile yield of PC occurs at $\sigma_{fy} = 62$ MPa; this is followed by a load drop to 52 MPa and a subsequent drawing of the material (accompanied with mild strain-hardening) until tensile fracture occurs at a nominal strain value of $\varepsilon \approx 1.15$. In compression, PC has a yield strength of 81 MPa. A strong strain-hardening behaviour is observed at a nominal compressive strain above 0.2, see Fig. 2a.

The nominal stress versus nominal strain response of PVC H200 foam is shown in Fig. 2b. The Young's modulus of the foam is $E_c = 125$ MPa, based on the measured responses at a strain rate of 10^{-4} s^{-1}. Tensile fracture of the foam occurs at $\varepsilon \approx 0.14$ and at an ultimate tensile strength (UTS) of approximately 4.7 MPa for all values of strain rate shown in Fig 2b. The compressive yield strength of the PVC foam (at onset of yield) is $\sigma_{cy} = 3.2$ MPa, with progressive strain-hardening of the foam evident at nominal compressive strains greater than 0.1. The responses of PC and PVC are only mildly sensitive to strain rate in the range 10^{-4} s^{-1} to 10^{-2} s^{-1} , see Figs. 2a and b.

3. Finite Element analysis

Quasi-static finite element (FE) calculations were performed within ABAQUS/Explicit v6.14 to simulate the indentation response of the PC/foam bi-layer, and to aid interpretation of the experimental results. Thus, it is appropriate to outline the FE analysis prior to reporting the indentation results.

The FE mesh for both the PC face sheet and PVC foam substrate comprised of linear quadrilateral elements in plane strain (type CPE4R)[**]. Perfect adhesion was assumed between the face sheet and foam substrate. The loading punch (and roller) were modelled as rigid surfaces, and a frictionless contact was assumed between the punch and the face sheet. A graded FE mesh was employed to provide adequate resolution close to the punch. The face sheet had 10 elements across its section to capture the bending stress field; a sensitivity study was performed to ensure that this mesh refinement was adequate to give a converged indentation load versus displacement response. A symmetric half model was employed in the FE study with the bottom edge of the core fixed and the loading punch (and roller) prescribed with a vertical downward velocity. The punch velocity is chosen to be sufficiently small for the inertial effects to be negligible; the response obtained from the Abaqus/Explicit simulation is thus quasi-static.

The PC face sheet was modelled as an isotropic, rate-independent, von Mises solid with a true stress versus true strain response as shown in Fig. 3a. This curve is derived from

[**] It is recognized that much of the specimen during indentation is not in a state of plane strain. However, local to the punch (or roller), large strain gradients exist and the assumption of plane strain behaviour is reasonable. The low plastic Poisson's ratio of the foam further restricts the out-of-plane deformation of the foam in the indentation zone.

the measured response of PC face sheet in uniaxial tension (at a strain rate of 10^{-4} s^{-1}) upon assuming a bi-linear fit for the post-yield nominal stress versus nominal strain data of Fig. 2a. The elastic modulus and Poisson's ratio are taken as $E_f = 2$ GPa and $\nu_f = 0.3$, respectively, based on the measured values in uniaxial tension. The PVC foam is specified with an elastic modulus $E_c = 125$ MPa and Poisson's ratio $\nu_c = 0.3$. The post-yield behaviour of the foam was modelled using the crushable foam model in ABAQUS which allows for a dissimilar response of the foam in tension and compression; a detailed description of the constitutive model is given in Appendix A. The assumed uniaxial compressive response of the foam is plotted in Fig. 3b; this curve is a smooth spline fit of the measured response in uniaxial compression (at a strain rate of 10^{-4} s^{-1}) upon excluding the stress peak at the onset of yield. A perfectly-plastic response is assumed for foam under tension via a constant parameter k_2 as explained in Appendix A. For a choice of $k_2 = 2.2$, the uniaxial tensile yield strength from the FE simulation agrees with the measured uniaxial tensile strength (of 4.7 MPa) to within 3%, and this value is employed in all the FE simulations. Failure of PC and PVC was not included in the FE model. Rate sensitivity was also neglected for both PC and PVC.

4. Experimental results and interpretation by finite element predictions

4.1 Indentation by flat-bottom punch

The indentation responses are compared in Fig. 4a for a PC/foam bi-layer ($t = 1$ mm, $c = 100$ mm, $\ell = 400$ mm) and for a foam layer absent the PC top layer; in both cases the flat-bottom punch of $2a = 4$ mm was used at an indentation speed of $\dot{v} = 0.025$ mms^{-1}, as listed in the basic study I of Table 1. Measurements are displayed in Fig. 4a for the 3 repeat tests and reveal minimal scatter. Predictions from the FE calculations are included in Fig. 4a and they show good agreement with the measured indentation responses for both the bi-layer and the foam layer.

The presence of the PC face sheet has a major effect upon the initial collapse load and the subsequent hardening response, as follows. We shall show below that, for the case of the PC/foam bi-layer, the high hardening rate is due to the development of tensile membrane stresses in the PC layer (first elastic stretching and then plastic stretching). It is less obvious why the indentation of an elastic, almost perfectly-plastic foam substrate (absent a PC top layer) leads to the strong hardening observed in Fig. 4a. An explanation is found in the fact that the foam cracks into a wedge-shaped crush zone beneath the indenter, see Fig. 4b. With increasing indent depth, the width of the crush zone increases in a linear fashion, and, upon assuming a constant magnitude of the local crush strength, the load increases with depth in a linear fashion. The measurements of Fig. 4a support this interpretation. We note in passing that there is a small discontinuous drop in load when a crack nucleates and propagates into the foam at an indentation depth of approximately 5 mm.

The measured load versus displacement response of a representative PC/foam bi-layer is replotted in Fig. 5a from the data of Fig. 4a, along with the analytical prediction (2) of Soden [13] for indentation of an elastic beam on a rigid, perfectly-plastic foundation. There is adequate agreement between the Soden [13] prediction and the initial post-yield response of the bi-layer. However, this analytical prediction becomes inadequate once $v > t = 1$ mm. We shall now show from DIC measurements and FE calculations that face sheet membrane stresses dominate the indentation response at deep displacements of the indenter relative to the face sheet thickness, and this is the root cause of the strong hardening behaviour.

In order to gain further insight into deep indentation, the distribution of von Mises strain ε_e (logarithmic) within the PC layer is determined by both DIC and FE analysis, for the bi-layer specimen of Fig. 5a at 3 stages of indentation: (A) $v = 0.5$ mm, (B) $v = 5$ mm and (C) $v = 12$ mm. These 3 values are marked in Fig. 5a and the strain distributions ε_e are given in Fig. 6. There is general agreement between the observed contours of strain from DIC and the FE prediction. The following broad remarks can be made from Fig. 5a and Fig. 6, taken together.

Load case A: At displacements $v << t = 1$ mm, the face sheet bends elastically with negligible membrane action, whilst the foam compresses in an elastic manner. Under increasing indentation, but $v/t < 1$, the foam substrate yields within a crush zone beneath the punch while the PC face sheet *bends elastically,* as idealised by Soden [13]. Yielding of the core in the FE simulations occurs at an indentation depth $v = 0.5$ mm, labelled as point A in Fig. 5a; the corresponding strain profile in the face sheet is shown in Fig. 6.

Load case B: When the displacement v is on the order of (or exceeds) the face sheet thickness t, the face sheet *stretches elastically* in addition to bending (in a plastic manner[††]) while the foam continues to compress in a plastic manner within the crush zone, as sketched in Fig. 5b. The strain profile in face sheet at point B corresponding to $v = 5$ mm is shown in Fig. 6. The face sheet has an almost constant curvature adjacent to the indenter and it carries a tensile load of magnitude T, as labelled in Fig. 5b.

Load case C: At displacements $v/t >> 1$, the tensile membrane stresses in the face sheet attain yield magnitude. With continued indentation, PC layer undergoes *plastic stretching*, and the magnitude of the plastic strain increases with increasing v. The deformed profile of the face sheet at point C (corresponding to $v = 12$ mm) resembles that of Fig. 5b, except $T = T_u = \sigma_{fy} t$ for this case. The strain profile recorded from the DIC is shown in Fig. 6 along with the FE prediction. Recall that the logarithmic failure strain of the PC (about 0.76) significantly exceeds that of the foam (about 0.13), and consequently the foam cracks adjacent to the stretched PC layer leading to a drop in the load at $v = 18.5$ mm.

[††] Note that the tensile yield strain of the PC is $\sigma_{fy}/E_f = 0.024$.

4.2 Role of indenter geometry and loading rate

A comparison of the measured load P versus displacement v response of the PC/foam bi-layer is given in Fig. 7a for the flat-bottom punches and circular rollers, at an indentation speed of 0.025 mms^{-1}; these are cases II and III of Table 1. Scatter was minimal and so only a representative P versus v response is shown in Fig. 7a. The predictions from the FE calculations are included in Fig. 7a and they show good agreement with the measured response for each case. We note from Fig. 7a that the P versus v responses are almost parallel for the flat-bottom punches and circular rollers, with an increase in load (for a given indent depth) with increasing a/t or r/t. In the flat-bottom punch tests, the peak load is dictated by cracking of the underlying foam, followed by shear-off of the PC from the corners of the punch, see Figs. 8a and b. The failure mode for the small circular roller is similar to that of the flat-bottom punch, see Fig. 8c. In contrast, at high r/t, first failure is by tensile cracking of the foam at the edge of the indentation zone, as shown in Fig. 8d. Punch velocity has only a minor effect upon the indentation response (study IV of Table 1), as shown in Fig. 7b for the flat-bottom punch of $a/t = 2$. This is attributed to the small strain rate sensitivity of both the PC face sheet and PVC foam.

4.3 Role of specimen length

The ability to develop membrane stresses relies upon load transfer between the face sheet and core over a shear lag zone adjacent to the crush zone, as sketched in Fig. 5b. Assume that the foam exerts a shear traction on the PC face sheet of magnitude equal to the shear yield strength τ_{cy} of the foam. Then, the length of shear lag zone ℓ_S in order to develop a membrane tension T in the PC face sheet equal to its yield value T_u $(= \sigma_{fy} t)$ is $\ell_S = \sigma_{fy} t/\tau_{cy} = 19$ mm for $\tau_{cy} = 2.7$ MPa. We anticipate that membrane stress is not able to develop to full extent when the semi-length of the bi-layer specimen is much less than this shear lag length. In order to confirm this, tests (of type V in Table 1) were performed on specimens of length $\ell = 50$ mm and 400 mm, using a flat-bottom punch of width $a/t = 2$, see Fig. 9. The initial indentation response is almost insensitive to the magnitude of ℓ for shallow indents such as $v < 2$ mm. However, at deep indents, such as $v > 5$ mm, the indentation load (at a given indent depth) for a specimen of $\ell = 50$ mm is significantly below that for $\ell = 400$ mm. An analytical model is now developed, based on the existence of the shear lag zone in order to predict the deep indentation resistance of the bi-layer .

5. Analytical model

Existing models for the indentation of sandwich beams assume that the indent depth is sufficiently small such that the face sheet behaves in a bending manner with negligible membrane action. In the present study, the indent depth increases to more than the face sheet thickness, and so significant membrane stresses develop in the face sheet: a new model is needed to account for this mode of deformation.

Consider plane strain indentation of a face sheet and underlying foam core by a flat-bottom punch of width $2a$, as shown in Fig. 10a. The face sheet is an elastic, perfectly-plastic solid, of plane strain Young's modulus E_f, tensile yield strength σ_{fy} and thickness t. It is perfectly adhered to a semi-infinite foam substrate. The foam core is treated as an elastic, perfectly-plastic solid of plane strain Young's modulus E_c, and compressive yield strength σ_{cy}.

The above experiments and FE analysis both suggest the following overall deformation mode. Assume that the face sheet develops a purely membrane state with a line tension (per unit length into the page), $T(x) = \sigma_f(x)t$ where $\sigma_f(x)$ is the tensile axial stress at any location x in the current configuration, see Fig. 10b. There are two distinct zones:

(i) an *outer shear lag zone* whereby the tension in the elastic face sheet drops with increasing x by the presence of a shear stress $\tau(x)$ on its lower face (adhered to the elastic foam substrate). This outer zone starts at a distance s from the centre line, see Fig. 10b.

(ii) an *inner zone of core crush* such that the foam core exerts a compressive normal traction of magnitude σ_{cy} on the underside of the face sheet in the deformed configuration. Since the shear traction of the foam core on the face sheet is negligible in this zone (of width $2s$) the tension $T(x)$ is uniform within this zone, and we write $T(x) = T_u$ for $a < |x| < s$. Force equilibrium of the membrane dictates that its radius of curvature R is given by

$$R = \frac{T_u}{\sigma_{cy}} \tag{7}$$

and we conclude that R is constant. Thus, the face sheet adopts the profile of a circular arc. We shall assume initially that the face sheet is elastic, but later extend our solution to the case where the face sheet yields at an axial tension $T_u = T_y$.

5.1 Indentation with elastic stretching of the face sheet

The core crush zone: Consider indentation to a depth v by the flat-bottom punch (of corner radius $\rho \ll a$). The load P is obtained by invoking vertical equilibrium to give

$$P = 2\sigma_{cy}(R\sin\omega + a) \tag{8}$$

where ω is the inclination of the face sheet adjacent to the punch, as defined in Fig. 10a. Geometry dictates that

$$v = R(1 - \cos\omega) \tag{9a}$$

and

$$s = R\sin\omega + a \tag{9b}$$

It remains to solve for R or equivalently the magnitude of T_u within the core crush zone, recall (7). To proceed, we turn our attention to the outer shear lag zone in order to solve for T_u.

Formulation for the outer shear lag zone: The membrane force T_u is resisted by both the face sheet and the underlying elastic core, and gives rise to an inward displacement u at the boundary $x = \pm s$ between core crush zone and outer shear lag zone, see Fig. 10c. This subsidiary problem gives us the spring constant k where

$$T_u = ku \tag{10}$$

First, we complete our analysis and then we present a finite element solution for the subsidiary problem of evaluation of k.

We assume that the face sheet remains bonded to the foam core, with vanishing slip, and that it undergoes negligible straining directly beneath the punch. At any indentation depth v, the face sheet elongates by 2χ over its length, where

$$\chi = \frac{T_u}{E_f t} R\omega + u \tag{11}$$

Upon comparing the initial and final configurations, χ is also given by

$$\chi = R\omega - R\sin\omega \tag{12}$$

Now, substitute (7), (10) and (12) into (11) to obtain

$$\omega - \sin\omega = \left(\frac{R\omega}{E_f t} + \frac{1}{k}\right)\sigma_{cy} \tag{13}$$

We emphasize that $k = k(s)$, and it is still to be found. Treat ω as the independent variable. Then, R is an implicit function of ω, and iteration is needed to solve (13) for R as a function of ω. After obtaining $R(\omega)$ we solve for the load $P(\omega)$ via (8), and thereby determine $v(\omega)$. The effective stiffness $k(s)$ is now obtained by solving a subsidiary problem using finite element analysis.

Finite element estimate for the spring stiffness k: The spring stiffness $k(s)$ in the outer shear lag region is estimated from the response of a force dipole of magnitude T_u in the face sheet, separated by a distance $2s$, as shown in Fig. 10c. The face sheet and the core in the outer shear lag region are assumed to behave as elastic solids with plane strain moduli E_f and E_c, respectively. The portion of the core within the crush zone has negligible stiffness and this is accounted for by the removal of a semi-circular portion of radius s from the core, as shown in Fig. 10c.

The FE calculations are performed using ABAQUS Standard (v6.14). Symmetry boundary conditions applied to one half of the FE model are shown in Fig. 11a. A 2D FE mesh is generated with ten 8-noded biquadratic plane strain elements (type CPE8R) along the thickness of the face sheet. A horizontal displacement u is applied to the vertical edge of the face sheet, and the value of the spring stiffness $k = T_u/u$ is computed for selected values of $E_f t/E_c s$ in the range of 0.1 to 10. A regression analysis for values of core depth $c \geq 10E_f t/E_c$ and specimen length $\ell \geq 2s + 10E_f t/E_c$ reveals power-law scaling between the spring constant k and (E_f, E_c, t, s) of the form

$$k = \beta E_c \left(\frac{E_f t}{E_c s}\right)^{1/3} \tag{14}$$

where $\beta = 0.36$, see Fig. 11b.

The dipole problem considered above additionally informs us of the length of shear lag zone. The shear traction $\tau(\xi)$ along the face sheet decays quadratically with distance ξ in the far-field region($\xi \gg s$), see Fig. 11c. A regression analysis for $\tau(\xi)$ in this region reveals a power-law scaling with $E_f t/E_c s$ as

$$\frac{s\tau(\xi)}{T_u} = 0.85 \left(\frac{s}{\xi}\right)^2 \left(\frac{E_f t}{E_c s}\right)^{2/3} \tag{15}$$

We define (arbitrarily) the shear decay length λ as the distance over which the shear traction decays to 1% of T_u/s, such that $\tau(\xi = \lambda) = 0.01T_u/s$. Accordingly, (15) gives an estimate for λ as

$$\frac{\lambda}{s} = 9.22 \left(\frac{E_f t}{E_c s}\right)^{1/3} \tag{16}$$

The value of λ as obtained from FE simulations for different values of $E_f t/E_c s$ in the range of 0.1 and 10 is plotted in Fig. 11d along with the predicted value (16); the agreement is excellent.

5.2 Comparison of analytical model with full indentation solution

A comparison of the indentation response from the above analytical model and from the full FE solution is given in Fig. 12a, for the case of a PC layer (t =1 mm) on a PVC foam substrate[‡‡] indented by a flat-bottom punch of width $2a$ = 1 mm . The substrate is of thickness c =1 m and of length ℓ = 1 m. We find from Fig. 12a that the P versus v responses are almost parallel, but there is an offset such that the analytical solution is stiffer. This is traced to the elastic compliance of the substrate in the FE model: it contributes an additional displacement Δv in the far-field region of magnitude

[‡‡] Note that the analytical model employs the plane strain values of Young's moduli for the PC face sheet (E_f = 2.2 GPa) and foam core (E_c = 137 MPa).

$$\Delta v = \frac{P}{2\pi E_c}\frac{3-4\upsilon_c}{1-\upsilon_c}\ln\left(\frac{c}{\lambda_o}\right) \tag{17}$$

as given by the standard Flamant solution [31] for the vertical displacement at a depth c due to a point transverse load P acting on the surface of an elastic solid with plane strain modulus E_c and Poisson's ratio υ_c. The characteristic length λ_o is taken to be $\lambda_o = E_f t/E_c$. The predicted response from the model upon accounting for the additional displacement (17) due to a finite core depth is close to the full FE response, see Fig. 12a.

Additional comparisons are made in Fig. 12b for the displacement profile of the top layer of the face sheet for $v = 10$ mm and in Fig. 12c for the decay of shear traction along the bottom layer of the face sheet, also for $v = 10$ mm. The face sheet displaces approximately in the form of a circular arc within the core crush zone as predicted by the model, see Fig. 12b. The shear traction along the face sheet in the outer shear lag region also shows good agreement with the prediction (15), as shown in Fig. 12c. It is further seen from Fig. 12d that the extent of the core crush zone s, as assumed in the force dipole problem for the computation of spring stiffness k, is approximately the plastic zone size in the full FE calculation. It appears that the force dipole problem, as depicted in Fig. 11a, is adequate to capture the response in the outer shear lag region.

5.3. Plastic stretching of the face sheet

At a sufficiently high load, the tension T_u in the face sheet within the inner zone of core crush attains the yield value $T_u = \sigma_{fy} t$. Consequently, (7) becomes

$$R = \frac{\sigma_{fy}}{\sigma_{cy}} t \tag{18}$$

and, upon substitution of this value for R into (13) and (14) along with (9b) we obtain a characteristic equation for the critical value of $\omega = \omega_y$ at the onset of plastic stretching of the face sheet as

$$\left(\frac{\sigma_{fy}}{\sigma_{cy}}\sin\omega_y + \frac{a}{t}\right)^{1/3}\left(\frac{E_f}{E_c}\right)^{2/3} - \beta\frac{E_f}{\sigma_{cy}}\left[\omega_y\left(1-\frac{\sigma_{fy}}{E_f}\right) - \sin\omega_y\right] = 0 \tag{19}$$

The value of the indentation load at the onset of plastic stretching in the face sheet P_y is obtained by substituting R from (18) and ω_y from (19) into (8) as

$$P_y = 2(\sigma_{fy} t\sin\omega_y + \sigma_{cy} a) \tag{20}$$

If the face sheet behaves in an elastic, perfectly-plastic manner, then necking will occur soon after T_u attains the value $\sigma_{fy} t$, and the limit load P_y is given by (20). In reality, PC has a sufficiently strong strain hardening characteristic beyond initial yield that it does not fail by necking but by cracking at an axial true strain on the order of 0.7. A more complex analytical model could be developed for the PC in the plastic range but this is beyond the scope of the present study and is of limited value.

The prediction of the above analytical model for the bi-layer geometry (and loading) of the basic study I of Table 1 is shown in Fig. 4a to compare with the measured response and the full finite element prediction (including the plastic response of PC face sheet). It is clear from Fig. 4a that the analytical model is in good agreement with measurement and FE prediction up to (and slightly beyond) the yield load P_y as given by (20)[§§]. At higher loads, the analytical model is somewhat too stiff and this is due to the fact that it neglects tensile yield of the face sheet.

The failure of both PC and PVC in the experiments occurs in the *plastic* stretching regime, as shown in Fig. 5. The analytical model, however, is developed for the bi-layer response during the *elastic* stretching of the face sheet which much precedes plastic stretching. This simple model also provides direct insight into the development of an elastic shear lag region between the face sheet and core. Additional finite element simulations were performed to verify the fidelity of the above analytical model over a wide range of bi-layer geometry (not shown here for brevity). We find that it suitably captures the elastic stretching of the face sheet and the shear lag between face sheet and core for $c \geq 10E_f t/E_c$ and $\ell \gg 10E_f t/E_c$, consistent with (14).

6. Indentation response of sandwich beam in 3-point bending

Is the indentation response of a bi-layer the same as that for a beam in 3-point bending, for the case where the beam collapses by an indentation mode? This is implicitly assumed to be the case in indentation analysis of sandwich beams. In order to address this question for the case of a PC/foam bi-layer, additional experiments were performed to compare the indentation response of a PC/foam sandwich beam in 3-point bending, with the indentation response of the bi-layer on a rigid support.

A typical 3-point bend geometry is shown in Fig. 13a. It comprises two identical PC face sheets of thickness t and a PVC foam core of thickness c. The sandwich beam is of depth b (into the page) and of span ℓ, and it is supported on its span by two circular rollers, each of radius R. Consider indentation of the beam by a flat-bottom punch of width $2a$ (with a corner radius ρ). We choose a geometry such that the beam collapses by plastic indentation; one such geometry is identified in Fig. B1 of Appendix B from a consideration of the competing collapse modes of indentation, face yield and core shear. Experiment and FE simulation were conducted on this beam of $\ell = 66$ mm, $c = 20$ mm, $t = 1$ mm and $b = 25$ mm. Support rollers of radius $R = 9.5$ mm, and a flat-bottom punch of width $2a = 4$ mm (with $\rho = 0.5$ mm) were employed. The punch speed was $v = 0.025$ mms^{-1}.

[§§] Note that the value of P_y as given by (20) is strictly conservative as it does not include the role of strain-hardening of PC and PVC present in the experiment and FE simulation.

The corresponding bi-layer geometry is given in Fig. 1: it has the geometry of the basic study I of Table 1, such that $t = 1$ mm, $c = 100$ mm and $\ell = 400$ mm. The load versus displacement responses of both specimens are given in Fig. 13b. The initial elastic response of both geometries is similar, with elastic bending of the face sheets and elastic compression of the core directly beneath the punch. Now consider each geometry in turn.

a) For the bi-layer case, the core yields beneath the punch and the face sheet bends elastically as suggested by the Soden solution (2) for small indent depth. Under increasing indent depth, membrane tension develops in the face sheet and this leads to a strong hardening response, as discussed above for the bi-layer problem.

b) For the sandwich beam, plastic collapse is by indentation of the top face sheet as suggested by Ashby et al. [8], with the formation of plastic hinges adjacent to the punch as shown in Fig. 14a. Both experiment and FE analysis reveal that indentation continues in the manner as shown in Fig. 13c for $v = 10$ mm; the measured and predicted deformation profile of the beam are in good agreement. We deduce from Fig. 13c that the post-yield indentation of the beam involves rotation of the two face sheets (by an angle ω) and transverse compression of the core (by an amount v_c), with negligible hardening in the load versus indent depth curve. The FE solution also reveals that membrane tension does not develop in the upper face sheet, consistent with the observation that the load versus indent depth curve is almost flat. This is explained in the following analytical model.

6.1 Analytical model for 3-point bending response

Consider the sandwich beam of Fig. 13a loaded by a flat-bottom punch (of corner radius $\rho \ll a$). Assume that the face sheets and core behave as elastic, perfectly-plastic solids of plane strain Young's moduli E_f and E_c, and of yield strengths σ_{fy} and σ_{cy}, respectively. At small values of punch displacement $v \ll t$, both the face sheets and core behave in an elastic manner such that the load P increases linearly with v according to [8] as

$$v = \frac{P\ell^3}{48(EI)_{eq}} + \frac{P\ell}{4(AG)_{eq}} \tag{21}$$

where $(EI)_{eq}$ is the equivalent flexural rigidity and $(AG)_{eq}$ is the equivalent shear rigidity of the sandwich beam; these relate to the elastic moduli and cross-sectional dimensions of the beam as

$$(EI)_{eq} = \frac{E_f bt(c+t)^2}{2} + \frac{E_f bt^3}{6} + \frac{E_c bc^3}{12} \quad \text{and} \quad (AG)_{eq} = \frac{G_c b(c+t)^2}{2} \tag{22}$$

Here, G_c is the shear modulus of the core.

Indentation collapse of the beam occurs when plastic hinges form in the top face sheet (adjacent to the punch) while the underlying core yields in compression, as sketched in Fig. 14a. At a small indent depth, the collapse load is that given by (4), and the mode is that of Ashby et al. [8]. The outer hinges have a fixed separation λ, where

$$\lambda = t\sqrt{\frac{\sigma_{fy}}{\sigma_{cy}}} \tag{23}$$

as discussed in [8]. The finite element solution suggests that this collapse mechanism evolves into the finite displacement version as defined in Fig. 14b, motivated by the observations of Fig. 13c. It has the following features. The two segments of the top face sheet, each of length λ, rotate but do not stretch. Directly beneath the punch, the core yields hydrostatically while the bottom face sheet yields in axial tension. The top face sheet carries negligible axial stress. An upper bound calculation is now performed to estimate the collapse response of the beam.

Consider first the top face sheet. Define ϕ as the angle of rotation of each of the 4 plastic hinges in the top face sheet such that

$$\phi = \sin^{-1}\left(\frac{v_c}{\lambda}\right) \tag{24}$$

where v_c is the core compression at any given value of the punch displacement v, as defined in Fig. 13c.

Now consider the neutral axis of bending of the beam section comprising core and bottom face sheet, at the mid-span position. Place the neutral axis at a height z above the outermost fibre of the bottom face sheet. Then, axial force equilibrium on this section dictates that

$$t\sigma_{fy} + (z-t)\sigma_{cy} = [c-(z-t)]\sigma_{cy} \tag{25}$$

with solution

$$z = t + \frac{c}{2}\left(1 - \frac{t\sigma_{fy}}{c\sigma_{cy}}\right) \tag{26}$$

For the sandwich beam under consideration, (26) implies that $z \approx t$, and the longitudinal stress state on the cross-section of the beam at mid-span is sketched in Fig. 14c.

Kinematic consistency between the face sheets and core implies

$$v = v_c + \frac{\ell}{2}\tan\omega \tag{27}$$

for an angle of rotation ω of the beam section about its neutral axis of bending at the mid-span section, as sketched in Fig. 14b. Equating the horizontal contraction of the core and top face sheet gives

$$c\tan\omega = \lambda(1-\cos\phi) \tag{28}$$

The indentation load of the sandwich beam is determined by a work calculation along the same lines as that of Ashby et al. [8]. The external plastic work done by load P during an incremental punch displacement δv is

$$\delta W = P\delta v \tag{29}$$

This is balanced by the internal plastic work which includes the contribution from two modes of deformation:

(i) a *local* mode of deformation involving the rotation of 4 plastic hinges in the top face sheet, each by an angle $\delta\phi$, and transverse compression of the core between the outer hinges by an amount δv_{c}. The incremental local plastic work δW_{L} (per unit depth of the beam) is

$$\delta W_{\mathrm{L}} = 4M_{\mathrm{Pf}}\delta\phi + (2a+\lambda\cos\phi)\sigma_{cy}\delta v_{\mathrm{c}} \tag{30}$$

where M_{Pf} is the plastic moment of the top face sheet section, $M_{\mathrm{Pf}} = \frac{1}{4}\sigma_{fy}t^2$; and

(ii) a *global* mode of deformation wherein the beam section (of core and bottom face sheet) rotates about the neutral axis of bending by an angle $\delta\omega$. The incremental global plastic work δW_{G} (per unit depth of the beam) is

$$\delta W_{\mathrm{G}} = 2M_{\mathrm{P}}\delta\omega \tag{31}$$

where M_{P} is the plastic moment of the beam section given by

$$M_{\mathrm{P}} = \frac{1}{2}\sigma_{cy}c^2\left(1-\frac{v_{\mathrm{c}}}{c}\right)^2 \tag{32}$$

upon ignoring the minor contribution from the top face sheet.

The statement of work balance, $\delta W = \delta W_{\mathrm{L}} + \delta W_{\mathrm{G}}$, reads

$$P\left(\delta v_{\mathrm{c}} + \delta\omega\frac{\ell}{2}\right) = 4M_{\mathrm{Pf}}\delta\phi + (2a+\lambda\cos\phi)\sigma_{cy}\delta v_{\mathrm{c}} + 2M_{\mathrm{P}}\delta\omega \tag{33}$$

upon using the relations (29)-(31). Now define two non-dimensional terms $\bar{v}$ and $\bar{\lambda}$ as

$$\bar{v} = \frac{\frac{v_{\mathrm{c}}}{\lambda}}{\sqrt{1-\frac{v_{\mathrm{c}}^2}{\lambda^2}}} \quad \text{and} \quad \bar{\lambda} = \lambda\sqrt{1-\frac{v_{\mathrm{c}}^2}{\lambda^2}} \tag{34}$$

The indentation load (33) for small ω can be rewritten in terms of $\bar{v}$ and $\bar{\lambda}$ using (24), (27) and (28) along with (34) as

$$P\left(1+\frac{\ell\bar{v}}{2c}\right)=\frac{4M_{\mathrm{Pf}}}{\bar{\lambda}}+(2a+\bar{\lambda})\sigma_{cy}+\frac{2M_{\mathrm{P}}\bar{v}}{c} \tag{35}$$

The full P versus v collapse response is obtained from (27) and (35) upon treating $\bar{v}$ as a free parameter, and this is plotted in Fig. 13b together with the initial elastic response (21). We find from Fig. 13b that the simple analytical model gives mild softening in contrast to the plateau in load as observed in the experiment and FE simulation. This is partly attributed to the lack of hardening in both the face sheet and the foam core in the analytical model.

We emphasize that there is a marked contrast between the collapse response of a simply supported beam and an end-clamped beam. For the end-clamped case, membrane tension *can* develop in the face sheet, as noted by Tagarielli and Fleck [32]. They compared the response of simply supported and end-clamped beams in 3-point bending, and showed that the end-clamping leads to a hardening curve of indent load versus displacement, and that the hardening is geometric in nature and not material related.

7. Concluding remarks

The present study highlights the fact that a PC face sheet significantly elevates the indentation strength of a PVC foam substrate. The foam compresses plastically while the face sheet remains elastic until the indent is much deeper than the face sheet thickness. The increase in indentation load is first due to elastic bending and then due to elastic stretching of the PC face sheet. This is supported by detailed finite element simulations and an analytical model that is based on the idea of load diffusion. Our study also highlights the distinction between the indentation response of a bi-layer on rigid foundation and a sandwich beam in 3-point bending. Although the initial yield load is comparable for the 2 geometries, the subsequent hardening responses differ significantly. Finite element analysis and an idealized analytical model reveal that the lack of hardening in the sandwich beam is due to the low bending strength of the core and bottom face sheet.

Acknowledgements

We acknowledge financial support from the ERC MULTILAT, grant number 669764. This work was also supported by the Engineering and Physical Sciences Research Council, award number 1463953. The authors are grateful for the financial support from SABIC and the technical assistance from Dr. Martin van Es.

Appendix A: The constitutive model for PVC foam

The post-yield behaviour of the PVC foam substrate is modelled using the ABAQUS crushable foam model with volumetric hardening. This phenomenological model allows for a dissimilar response of the foam in tension and compression, as commonly observed in polymer foams such as PVC, see Fig. 2a. The yield surface is assumed to be elliptical, and of the form

$$\phi = \sigma_e^2 + \alpha^2(\sigma_m^2 - A^2) - B^2 \leq 0 \tag{A.1}$$

where σ_e is the von Mises effective stress, σ_m is the mean stress, and α is the shape factor of the yield ellipse. The parameters A and B scale with the hydrostatic compressive strength of the foam p_c and with the hydrostatic tensile strength p_t according to

$$A = \frac{p_c - p_t}{2} \qquad \text{and} \qquad B = \alpha\frac{p_c + p_t}{2} \tag{A.2}$$

In order to account for the observed value of zero plastic Poisson's ratio for the PVC foam, a non-associated plastic flow rule is adopted, with an assumed flow potential μ of the form

$$\mu = \sigma_e^2 + \frac{9}{2}\sigma_m^2 \tag{A.3}$$

During plastic flow, the hydrostatic compressive strength p_c increases with the increasing magnitude of the volumetric compressive plastic strain, while the hydrostatic tensile strength p_t remains constant. The hardening response of the foam is specified in the FE model by providing the uniaxial Cauchy stress versus true plastic strain data from a uniaxial compression test as shown in Fig. 2a.

The shape factor α of the yield surface is specified via the two strength ratios: (i) the ratio of the initial yield strength in uniaxial compression to hydrostatic compression, k_1, and (ii) the ratio of the yield strength in hydrostatic tension to the initial yield strength in hydrostatic compression, k_2. These are related to α according to

$$\alpha = \frac{3k_1}{\sqrt{(3k_2 + k_1)(3 - k_1)}} \tag{A.4}$$

The values of k_1 and k_2 are such that $0 < k_1 < 3$ and $k_2 > 0$. For the PVC H200 foam employed in this study, $k_1 \approx 2$ based on the experimental study of Deshpande and Fleck [33], and $k_2 = 2.2$ in order for the predicted uniaxial tensile strength for the foam to match the measured uniaxial tensile strength (to within 3%). Consequently, we obtain $\alpha \approx 2$ for the H200 foam.

Appendix B: Collapse modes of simply supported sandwich beams

The competing collapse modes of simply supported sandwich beams have been investigated by Ashby et al. [8] for metallic face sheets and core. These modes are classified as face yield, core shear, and indentation. The active collapse mechanism for a given set of geometrical parameters of the beam and material properties is the one that gives the lowest collapse load. Define the non-dimensional collapse load as $\bar{P} = P/b\ell\sigma_{fy}$. The expressions for $\bar{P}$ for each collapse load, as taken from [8], are given below in terms of the non-dimensional face sheet thickness, $\bar{t} = t/c$ and core thickness, $\bar{c} = c/\ell$, along with the relevant material properties of the face sheets and core such as the compressive yield strength and shear yield strength core, σ_{cy} and τ_{cy}, respectively, and the yield strength of the face sheet σ_{fy}.

Face yield: Plastic collapse occurs when face sheets attain the yield strength while the core yields simultaneously. The collapse load for face yield is

$$\bar{P} = \left[4\bar{t}(1+\bar{t}) + \frac{\sigma_{cy}}{\sigma_{fy}}\right]\bar{c}^2 \tag{B.1}$$

Plastic indentation: Plastic collapse occurs when plastic hinges form in the top face sheet adjacent to the loading punch while the core yields in compression, recall (4). The collapse load for indentation is re-cast in its non-dimensional form as

$$\bar{P} = 2\bar{t}\bar{c}\left(\frac{\sigma_{cy}}{\sigma_{fy}}\right)^{1/2} + \frac{2a}{\ell}\frac{\sigma_{cy}}{\sigma_{fy}} \tag{B.2}$$

Core shear: Plastic collapse occurs when plastic hinges form at the mid-span of the sandwich beam and at the outer supports, along with shear yielding of the core. The collapse load for core shear is

$$\bar{P} = 4\bar{t}^2\bar{c}^2 + 2\bar{c}\frac{\tau_{cy}}{\sigma_{fy}} \tag{B.3}$$

A plastic collapse mechanism map, with axes in the form of $\bar{t}$ and $\bar{c}$, can be constructed by making use of the relations (B.1) - (B.3) for selected values of the material properties. One such map for the choice of PC face sheets and PVC foam core, with $\sigma_{cy}/\sigma_{fy} = 0.06$ and $\tau_{cy}/\sigma_{fy} = 0.052$, and non-dimensional punch width $2a/\ell = 0.05$ is shown in Fig. B1. The collapse mechanism map of Fig. B1 does not contain a domain of 'adhesive debond' due to the fact that the adhesive employed in the present study is of adequate strength (and it is defect-free) such that complete adhesion is maintained between the face sheets and core during the course of the test.

References

[1] Andrews EW, Sanders W, Gibson LJ. Compressive and tensile behaviour of aluminium foams. Material Science and Engineering A 1999; 270(2):113-24.

[2] Jang , Kyriakides S. On the crushing of aluminium open-cell foams : Part I . Experiments. International Journal of Solids and Structures 2009; 46(3-4):617–34.

[3] Gaitanaros S, Kyriakides S. On the effect of relative density on the crushing and energy absorption of open-cell foams under impact. International Journal of Impact Engineering 2015; 82:3–13.

[4] Olurin OB, Fleck NA, Ashby MF. Indentation resistance of an aluminium foam. Scripta Materialia 2000; 43(11): 983–89.

[5] Flores-Johnson EA, Li QM. Indentation into polymeric foams. International Journal of Solid sand Structures 2010; 47(16):1987–95.

[6] Onck P, Andrews EW, Gibson LJ. Size effects in ductile cellular solids. Part I: Modeling results. International Journal of Mechanical Sciences 2001; 43(3):681–99.

[7] Andrews EW, Gioux G, Onck P, Gibson LJ. Size effects in ductile cellular solids. Part II: Experimental results. International Journal of Mechanical Sciences 2001; 43(3):701–13.

[8] Ashby MF, Evans AG, Fleck NA, Hutchinson JW, Gibson LJ, Wadley HNG. Metal foams: a design guide. London: Butterworth-Heinemann; 2000.

[9] Steeves CA, Fleck NA. Collapse mechanisms of sandwich beams with composite faces and a foam core, loaded in three-point bending. Part I: Analytical model and minimum weight design. International Journal of Mechanical Sciences 2004; 46:561–83.

[10] Mohan K, Tip YH, Sridhar I, Seow HP. Effect of face sheet material on the indentation response of metallic foams. Journal of Materials Science 2007; 42(11): 3714–23.

[11] Biot MA. On bending of an infinite beam on an elastic foundation. Journal of Applied Mathematics and Mechanics 1937; 22(5):984–88.

[12] Hetenyi M. Beams on elastic foundation. Waverly press, Baltimore, 1946

[13] Soden PD. Indentation of Composite Sandwich Beams. 1966; 31(5):353-60.

[14] Shuaeib FM, Soden PD. Indentation failure of composite sandwich beams. Composites Science and Technology 1997; 57(9–10):1249–59.

[15] Pitaarresi G. Indentation of rigidly supported sandwich beams with foam cores exhibiting non-linear compressive behaviour. Journal of Sandwich Structures and Materials 2011; 13(5):605-36.

[16] Bostrom PO. Collapse modes of a rigid-plastic beam on a rigid-plastic foundation. International Journal of Mechanical Sciences 1975; 17(1):73-84.

[17] Chen C, Harte AM, Fleck NA. Plastic collapse of sandwich beams with a metallic foam core. International Journal of Mechanical Sciences 2001; 43(6):1483–1506.

[18] Bart-Smith H, Hutchinson JW, Evans AG. Measurement and analysis of the structural performance of cellular metal sandwich construction. International Journal of Mechanical Sciences 2001; 43(8):1945–63.

[19] McCormack TM, Miller R, Kesler O, Gibson LJ. Failure of sandwich beams with metallic foam cores. International Journal of Solids and Structures 2001; 38:4901–20.

[20] Yu TX, Stronge WJ. Large deflections of a rigid-plastic beam-on-foundation from impact. International Journal of Impact Engineering 1990; 9(1):115-26.

[21] Rubino V, Deshpande VS, Fleck NA. The three-point bending of Y-frame and corrugated core sandwich beams. International Journal of Mechanical Sciences 2010; 52(3):485-94.

[22] Qin QH, Wang TJ. Plastic anlaysis of metal foam core sandwich beam transversely loaded by a flat punch: combined local denting and overall deformation. Journal of Applied Mechanics 2012; 79(4):1-12.

[23] Xiao D, Mu L, Zhao G. Influence of positive gradient metallic cellular core on energy dissipation of sandwich panels under indentation. Archive of Applied Mechanics 2016; 86:1901–11.

[24] Xie ZY, Yu JL, Zheng ZJ. A plastic indentation model for sandwich beams with metallic core. Acta Mechanica Sinica 2011; 27(6):963–66.

[25] Qin Q, Zhang J, Wang Z, Li H, Guo D. Indentation of sandwich beams with metal core. Transactions of Nonferrous Metals Society of China, 2014; 24: 2440-2446

[26] Zhang J, Qin Q, Ai W, Wang Z, Wang T. Indentation of metal foam core sandwich beams: Experimental and theoretical investigations. Experimental Mechanics 2016; 56(5):771–84.

[27] Zhang J, Qin Q, Wang Z, Ai W, Wang TJ. A theoretical study of plastic analysis of fully clamped geometrically asymmetric sandwich beams with a metal foam core. International Journal of Mechanical Sciences 2015; 99:98–111.

[28] Boyce AM, Deshpande VS, Fleck NA. On the indentation resistance of a PC layer on PVC foam substrate. Advanced Engineering Materials 2017; 19(10):1700075.

[29] Koiter WT. On the diffusion of load from a stiffener into a sheet. Journal of Applied Mechanics 1966; 3(2):164–78.

[30] Muki R, Sternberg E. Transfer of load from an edge-stiffener to a sheet — A

reconsideration of Melan's problem. Journal of Applied Mechanics 1967; 34(3):679–86.

[31] Johnson, KL. Contact Mechanics. Cambridge: Cambridge University Press; 1985.

[32] Tagarielli VL, Fleck NA, Deshpande VS. Collapse of clamped and simply-supported composite sandwich beams in three-point bending. Composites Part B 2001; 35(6-8):523-34

[33] Deshpande VS, Fleck NA. Multi-axial yield behaviour of polymer foams. Acta Materialia 2001; 49(10):1859–66.

Tables

		Specimen	a (mm)	r (mm)	$\dot{v}$ (mm/s)	ℓ (mm)
Basic study	I	Medium punch on PC/PVC foam bi-layer	2	-	0.025	400
		Medium punch on PVC foam layer	2	-	0.025	400
Indenter study	II	Small punch	1	-	0.025	400
		Medium punch	2	-	0.025	400
		Large punch	5	-	0.025	400
	III	Small roller	-	1	0.025	400
		Medium roller	-	2	0.025	400
		Large roller	-	5	0.025	400
Rate study	IV	Low rate	2	-	0.0025	400
		High rate	2	-	0.25	400
Length study	V	Short specimen	2	-	0.025	50
		Long specimen	2	-	0.025	400

Table 1. Geometry and experimental details of the indentation tests. In all cases, $t = 1$ mm, $c = 100$ mm, and $b = 25$ mm.

Figures

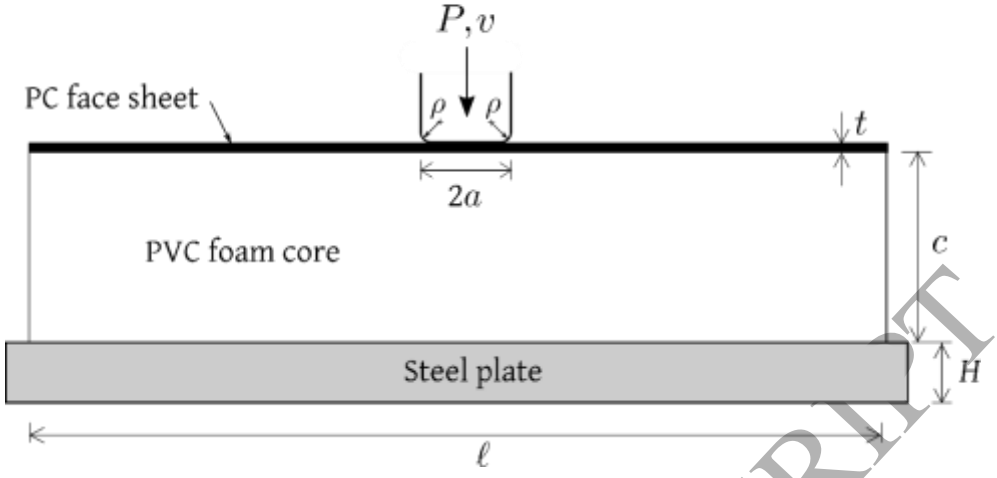

Fig. 1. Geometry and loading in indentation tests.

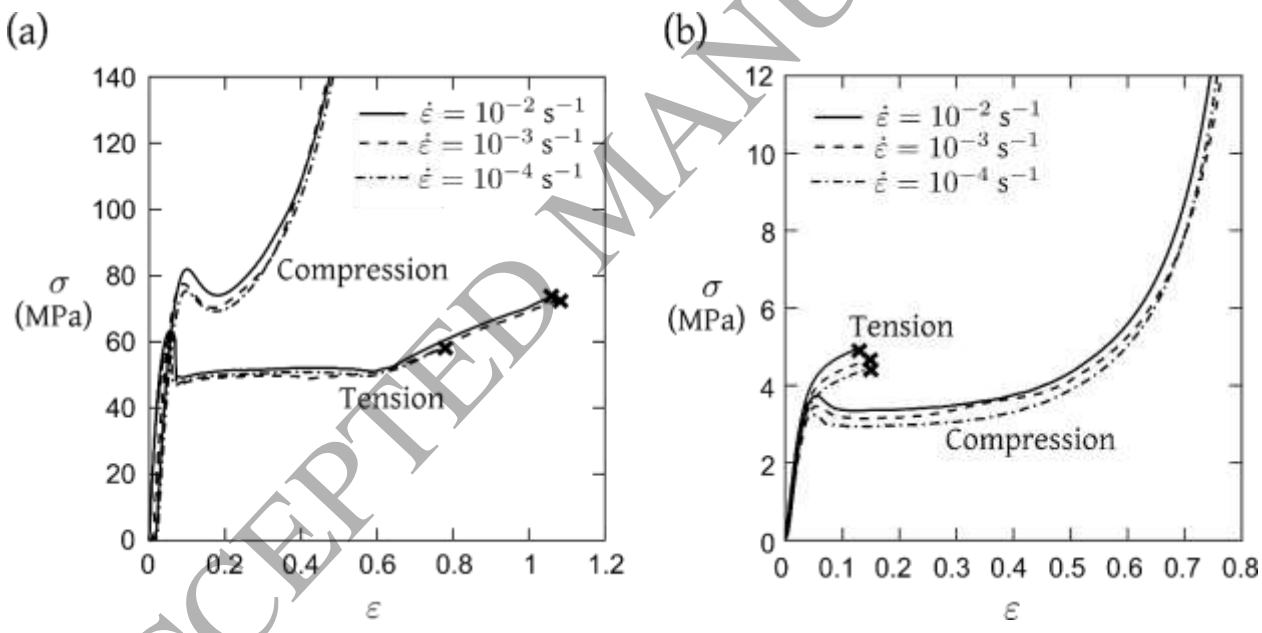

Fig. 2. Nominal tensile and compressive responses for **(a)** polycarbonate and **(b)** H200 PVC foam for strain rates of $10^{-4}s^{-1}, 10^{-3}s^{-1}$, and $10^{-2}s^{-1}$. Cross marks indicate failure.

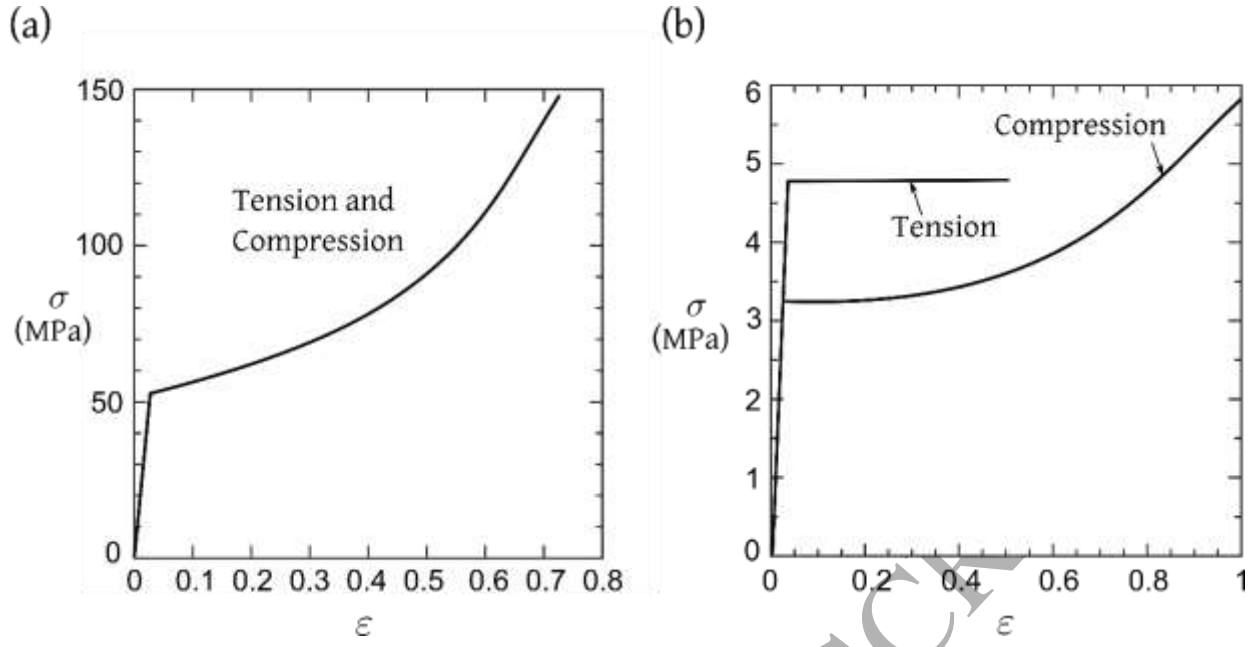

Fig. 3. Uniaxial true stress versus logarithmic strain responses for the FE simulations: **(a)** PC face sheet and **(b)** PVC H200 foam core.

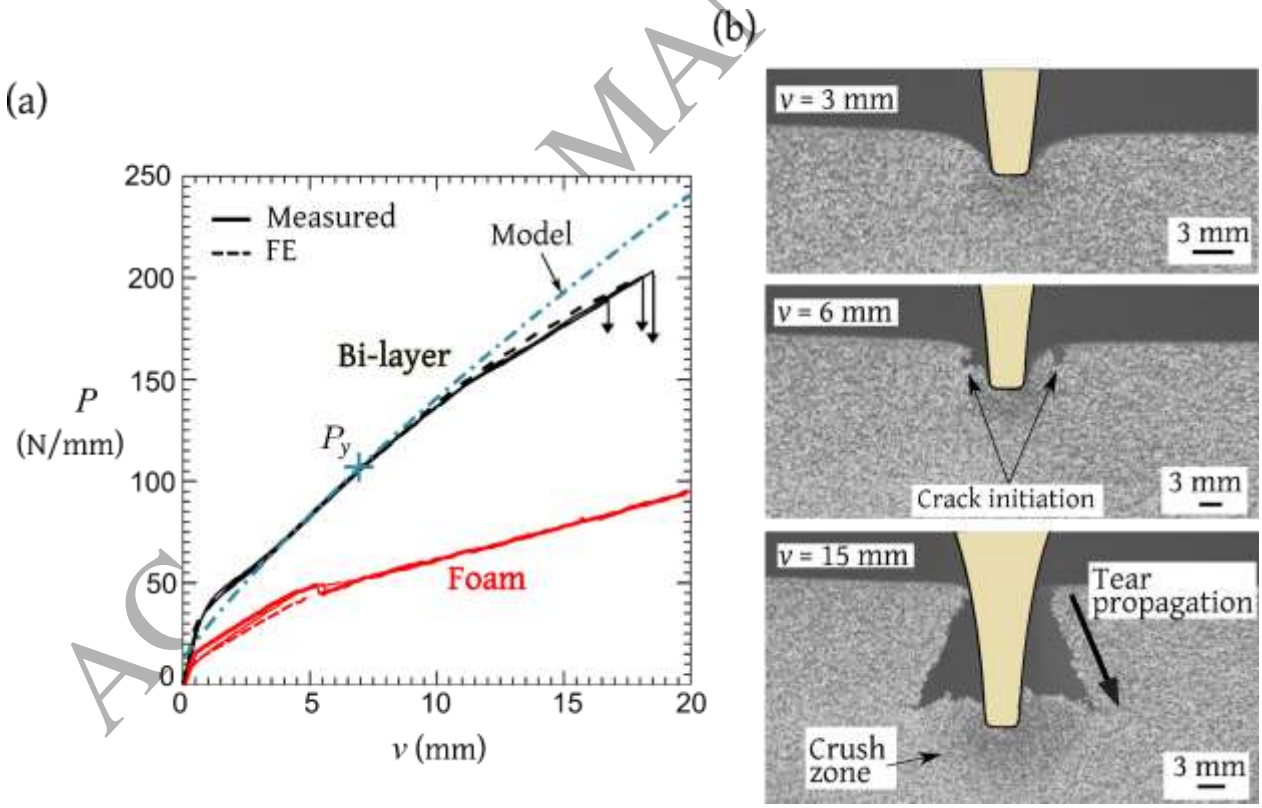

Fig. 4. Indentation response of PC/foam bi-layer and foam layer (Study I): **(a)** Load versus displacement response and **(b)** Observed damage progression in the foam.

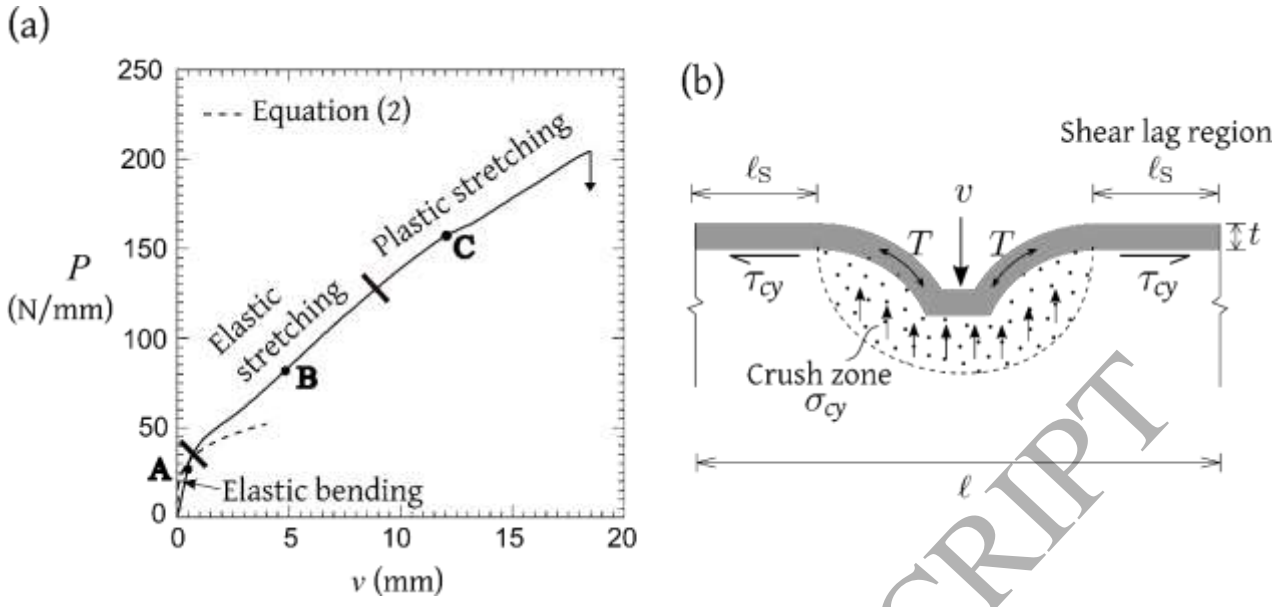

Fig. 5. **(a)** Indentation response of PC/PVC foam bi-layer (Study I). The boundary between elastic bending and elastic stretching at $v = 0.6$ mm and the boundary between elastic stretching and plastic stretching at $v = 8$ mm are taken from the corresponding FE solution of Fig. 4a. **(b)** Stretching of the face sheet during deep indentation.

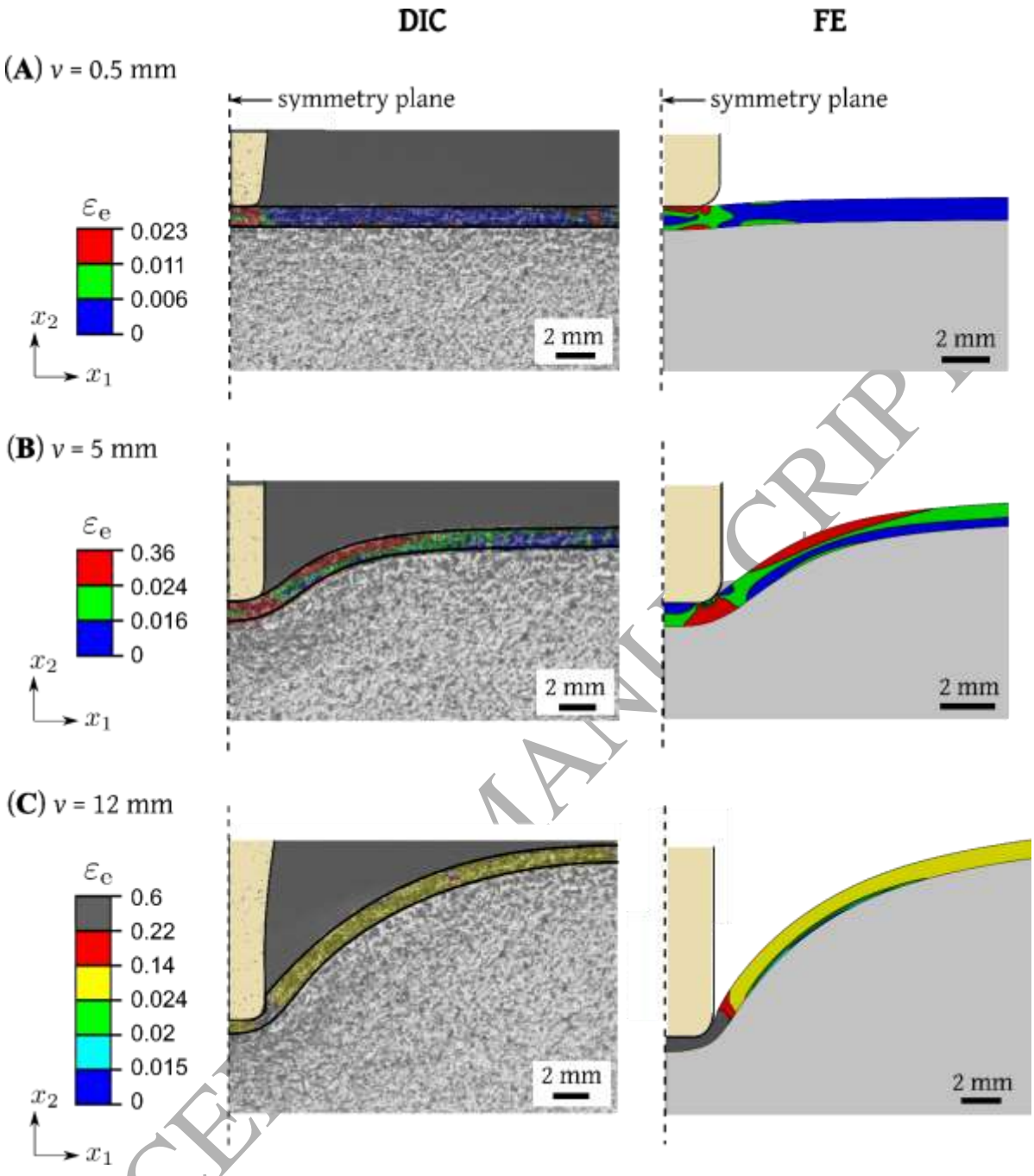

Fig. 6. Contours of von Mises strain in the PC face sheet of the bi-layer at increasing values of indent depth (Study I), at loads A, B, C as marked in Fig. 5a.

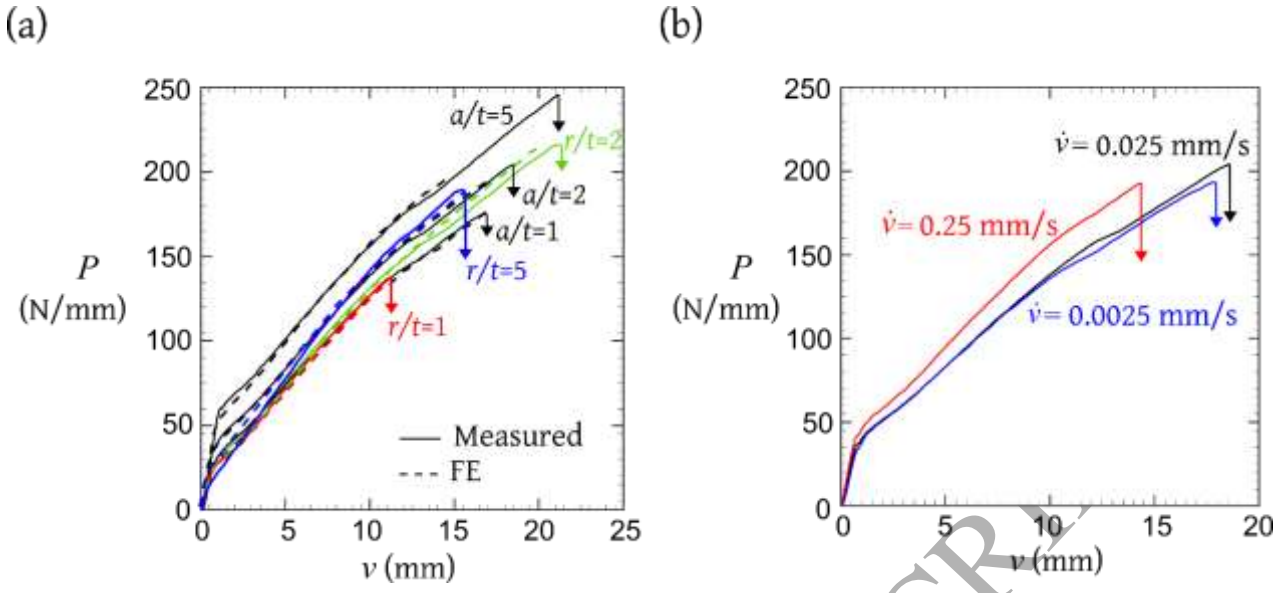

Fig. 7. (a) Load versus displacement response for (i) flat-bottom punch, width $a/t = 1,2,5$ (Study II) and, (ii) cylindrical roller, radius $r/t = 1,2,5$ (Study III) at an indentation speed $\dot{v} = 0.025$ mm/s, **(b)** Load versus displacement response for flat punch indentation ($a/t = 2$) at selected indentation speeds (Study IV).

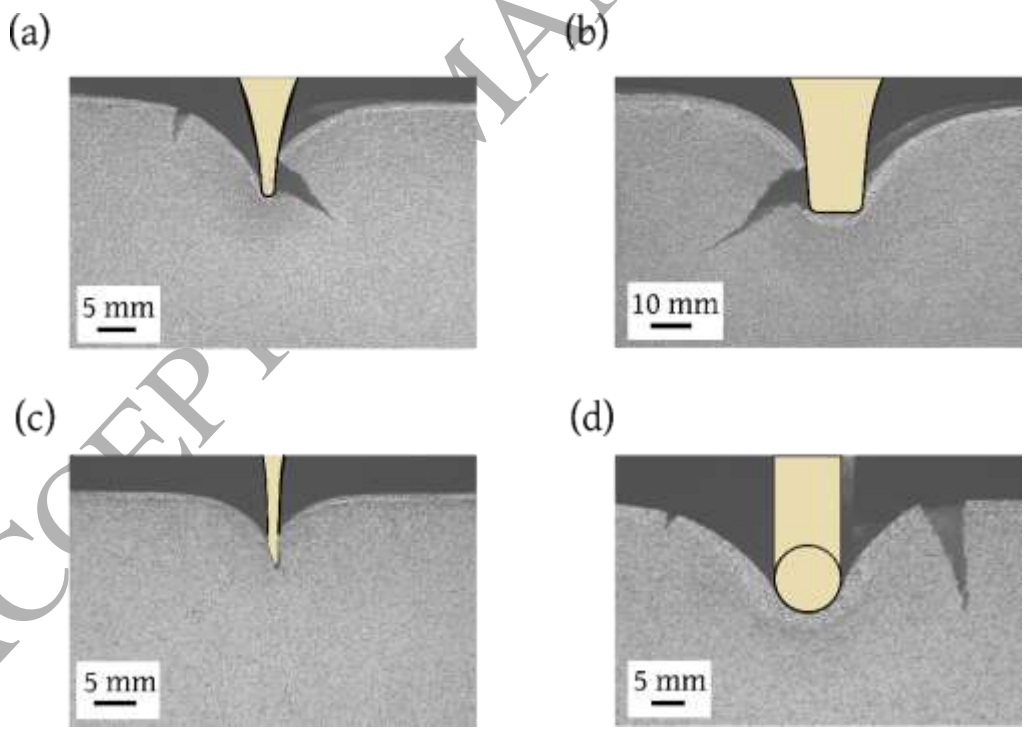

Fig. 8. Observed failure modes in the indentation of bi-layer with flat-bottom punches of **(a)** $a/t = 1$ at $v = 16.7$ mm and **(b)** $a/t = 5$ at $v = 21.2$ mm, and with cylindrical rollers of **(c)** $r/t = 1$ at $v = 11.5$ mm and **(d)** $r/t = 5$ at $v = 15.8$ mm.

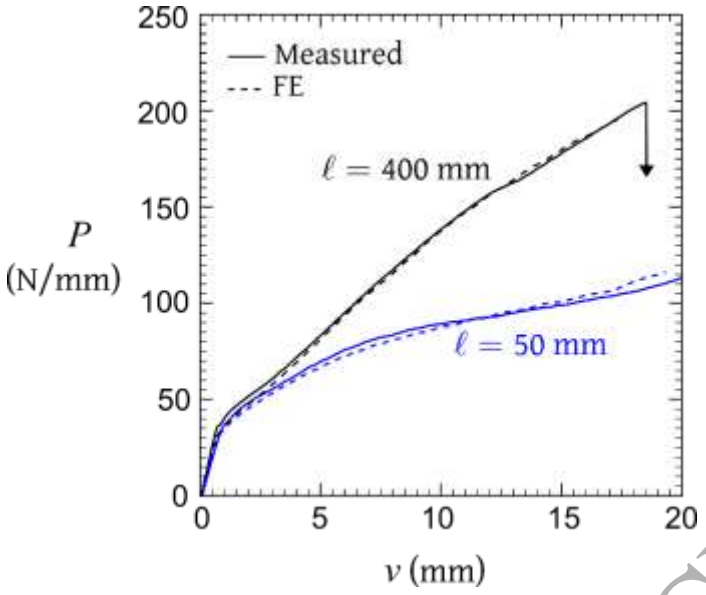

Fig. 9. Effect of specimen length on the indentation response of bi-layer (Study V).

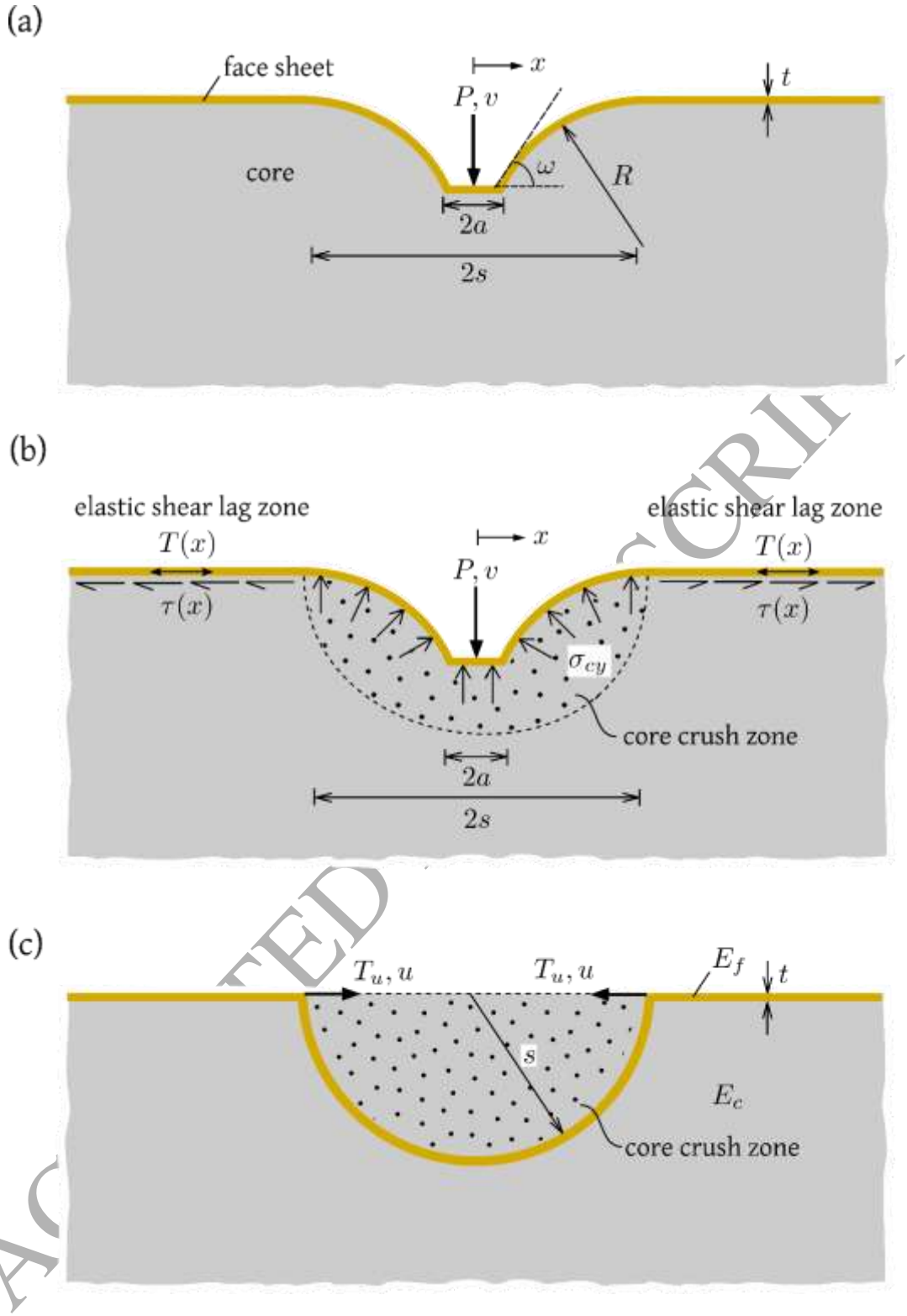

Fig. 10. Indentation of a face sheet attached to a foam core: **(a)** geometry and loading, **(b)** stress state in the face sheet and core under the applied loading, and **(c)** geometry and loading for the subsidiary problem of determining the elastic spring stiffness in the shear lag zone.

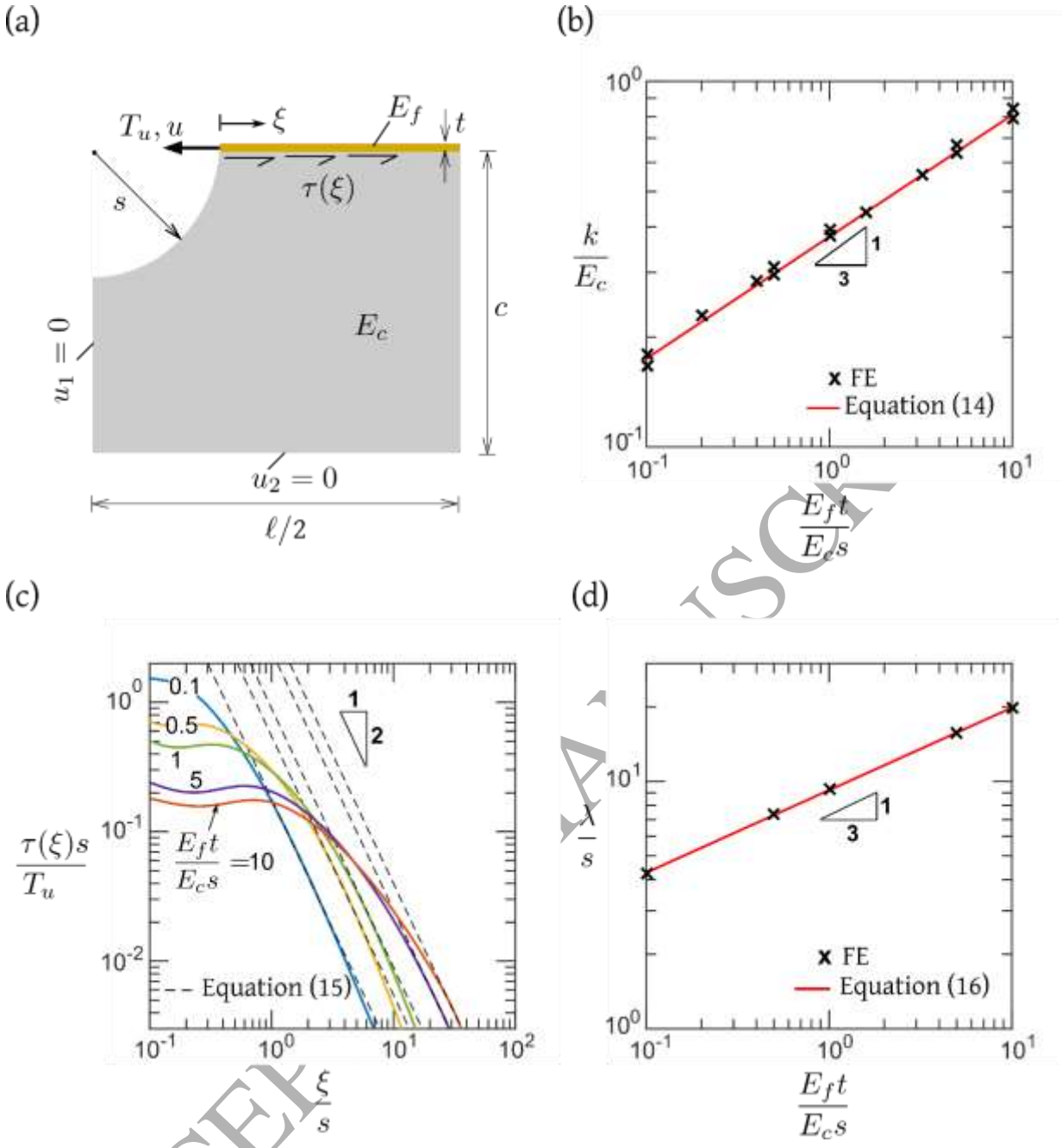

Fig. 11. Force dipole problem: **(a)** geometry and loading employed in the FE simulation, **(b)** scaling for the spring stiffness k, **(c)** shear traction on the bottom layer of the face sheet $\tau(\xi)$; solid lines are FE predictions, and **(d)** scaling for the shear lag length $\boldsymbol{\lambda}$.

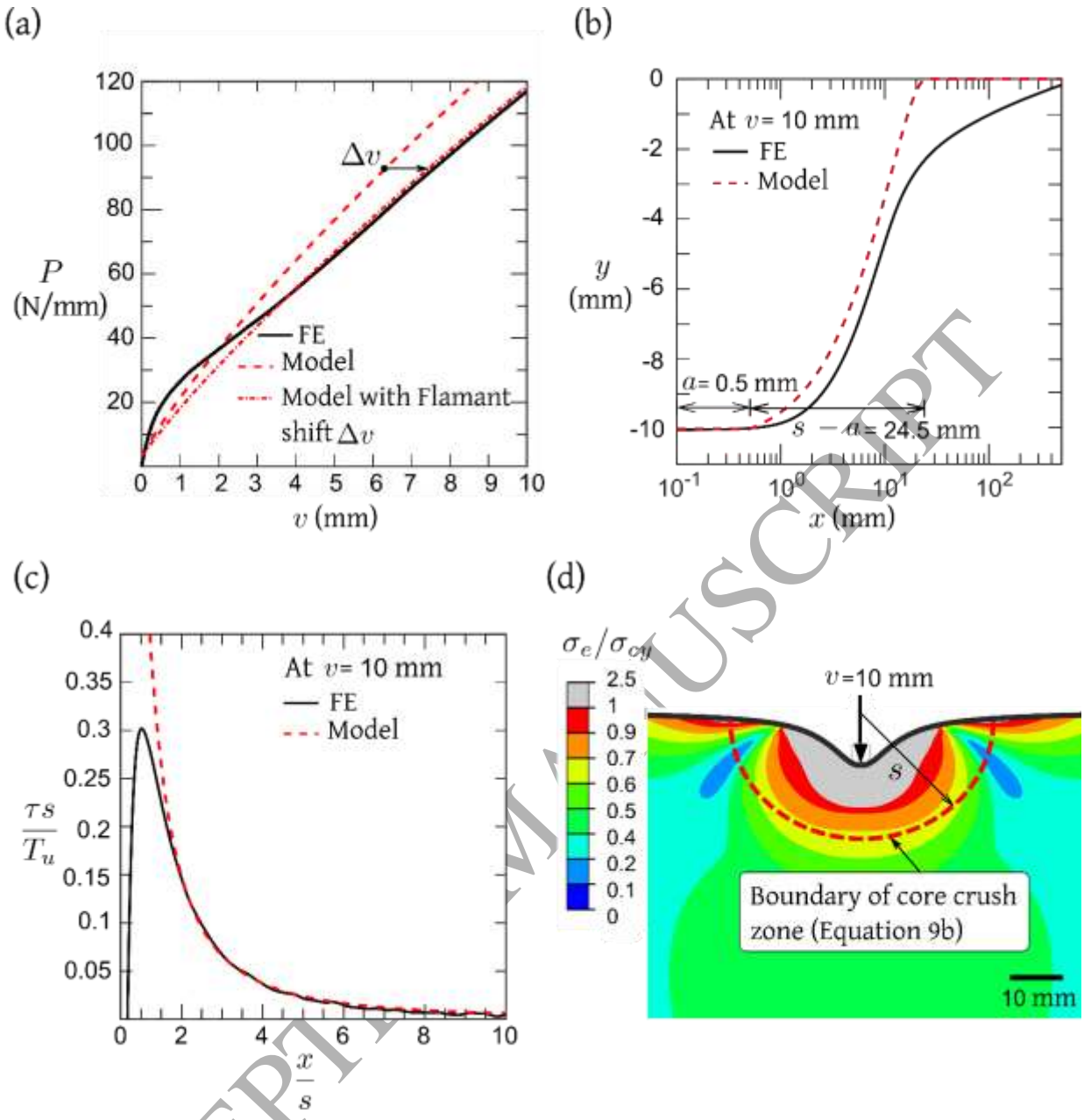

Fig. 12. Comparison of the elastic membrane model with the full FE indentation response (with elastic face sheet): **(a)** Load versus displacement, **(b)** displacement profile of the top layer of the face sheet, **(c)** shear traction on the bottom layer of the face sheet, and **(d)** contours of the von Mises stress in the foam core; **(b)**-**(d)** correspond to $v = 10$ mm.

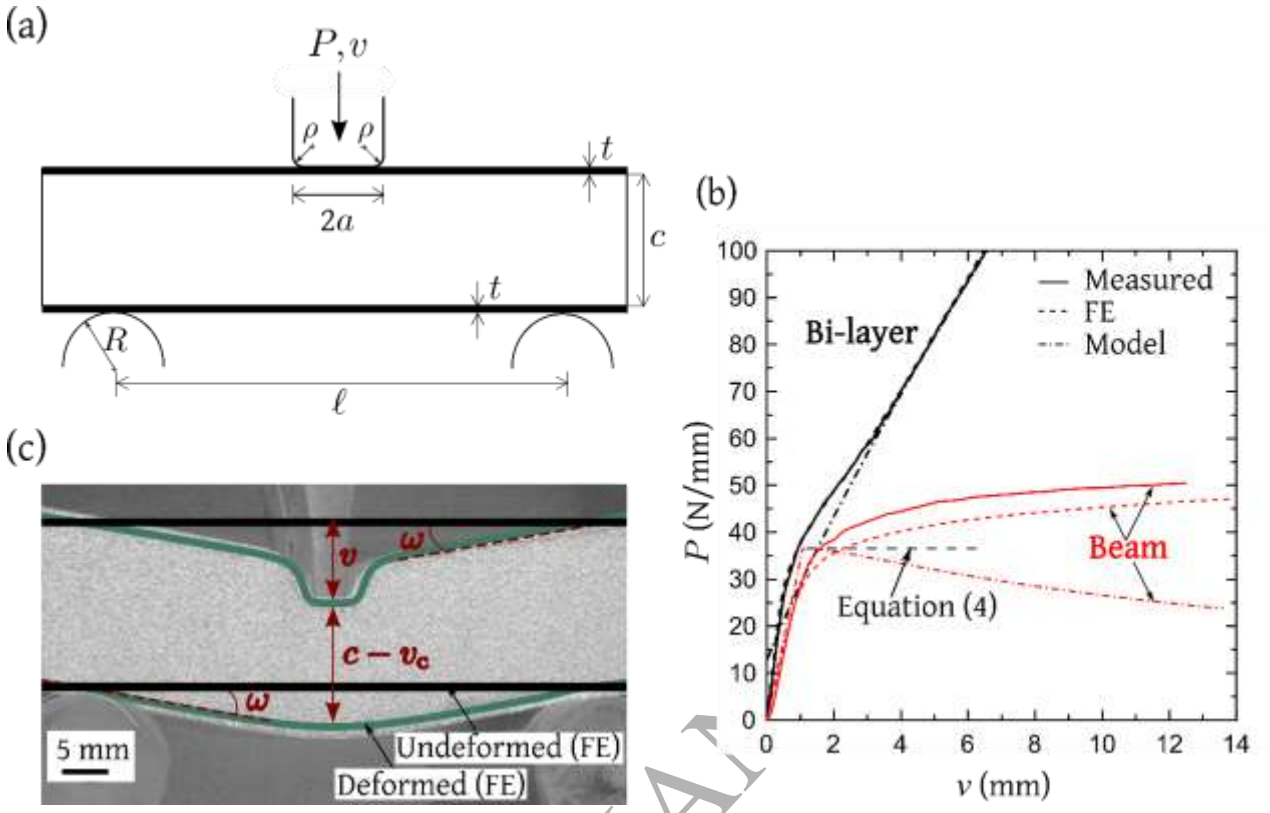

Fig. 13. Indentation response of a sandwich beam under 3-point bending: **(a)** geometry and loading, **(b)** load versus displacement response of the PC/PVC beam, and **(c)** an overlay of the observed deformation profile of the beam in the experiment and the predicted deformation profile from FE at $v = 10$ mm; only the face sheet deformation from the FE prediction is shown here.

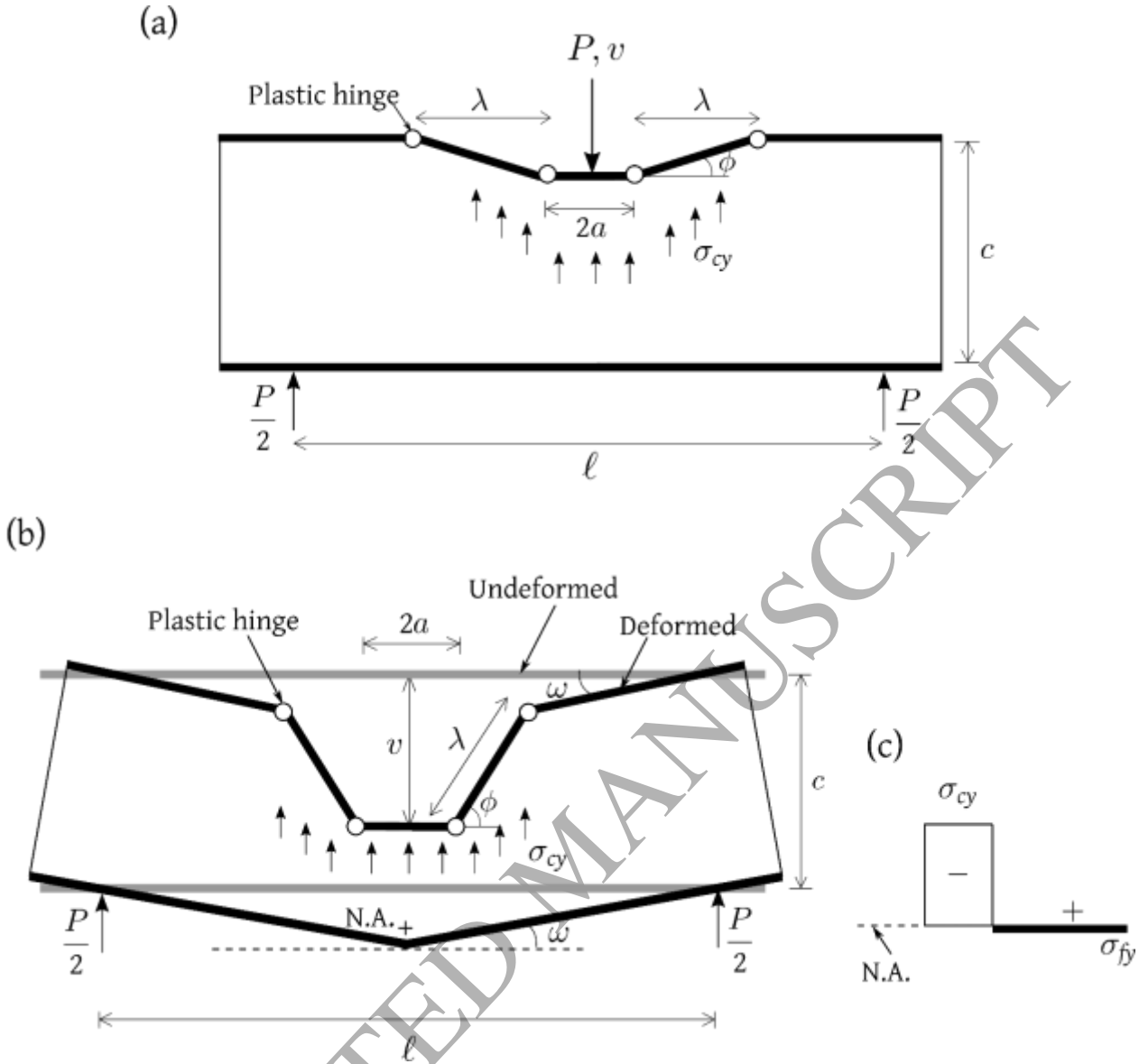

Fig. 14. Indentation collapse of a sandwich beam under 3-point bending: **(a)** Collapse mode at small punch displacement [8], **(b)** assumed collapse mode for finite punch displacement, **(c)** assumed distribution of the longitudinal stress in the core and bottom face sheet at the mid-span section of the beam. N.A. refers to the Neutral Axis of bending.

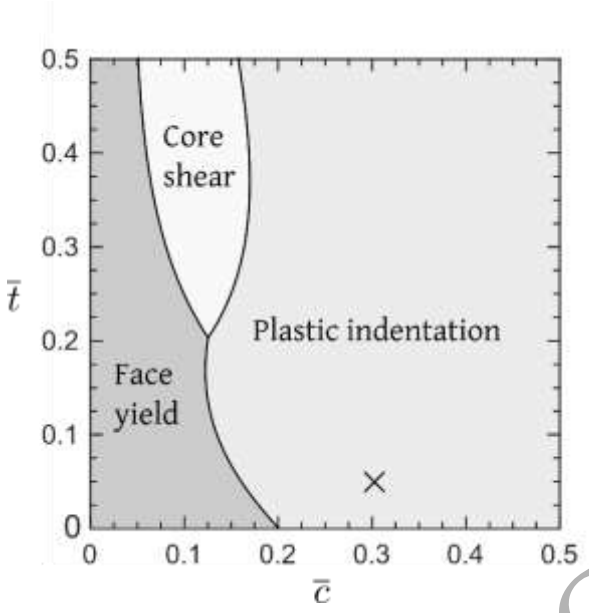

Fig. B1. Collapse mechanism map for a simply supported sandwich beam made from PC face sheets and PVC H200 foam core, and loaded by a flat-bottom punch of $2a/\ell = 0.05$. The data point x refers to the geometry of sandwich beam that was tested.

graphical abstract